Available online at www.sciencedirect.com

SciVerse ScienceDirect

Geochimica et Cosmochimica Acta 83 (2012) 205–216

Geochimica et Cosmochimica Acta

www.elsevier.com/locate/gca

As(III) immobilization on gibbsite: Investigation of the complexation mechanism by combining EXAFS analyses and DFT calculations

Graziele Duarte [a,g], Virginia S.T. Ciminelli [a,g,*], Maria S.S. Dantas [a,g], Helio A. Duarte [b,g], Igor F. Vasconcelos [c,g], Augusto F. Oliveira [d,g], Kwadwo Osseo-Asare [e,f,g]

[a] *Department of Metallurgical and Materials Engineering, Universidade Federal de Minas Gerais, Av. Antonio Carlos, 6627, Engineering School, Bloco 2, s/2233, Campus Pampulha, 31270-901, Belo Horizonte, Minas Gerais, Brazil*

[b] *Department of Chemistry, Universidade Federal de Minas Gerais, Campus Pampulha, Belo Horizonte, Minas Gerais, Brazil*

[c] *Department of Metallurgical and Materials Engineering, Universidade Federal do Ceará, Campus do Pici Bloco 714, CEP 60455-760, Fortaleza, Ceará, Brazil*

[d] *School of Engineering and Science, Jacobs University Bremen, Campus Ring 1, 28759 Bremen, Germany*

[e] *Department of Materials Science and Engineering, The Pennsylvania State University, University Park, PA 16802, USA*

[f] *Department of Energy and Mineral Engineering, The Pennsylvania State University, University Park, PA 16802, USA*

[g] *National Institute of Science and Technology on Minerals Resources, Water and Biodiversity: INCT-Acqua, Brazil*

Received 14 December 2010; accepted in revised form 7 November 2011; available online 19 December 2011

Abstract

The complexation of aqueous As(III) species on gibbsite was investigated as a function of pH. Theoretical calculations and X-ray absorption fine structure spectroscopy (XAFS) were combined to elucidate the structure of arsenite surface complexes on synthetic gibbsite. Several adsorption sites were evaluated using the self-consistent charge corrected density-functional based tight-binding (SCC-DFTB) method. The formation of bidentate–binuclear, bidentate–mononuclear, monodentate–mononuclear, and monodentate–binuclear complexes by means of both acid–base and non-dissociative mechanisms was studied in detail. The SCC-DFTB calculations showed the bidentate–binuclear/acid–base complex as the most thermodynamically stable geometry for As(III) bonding to gibbsite surface, estimating As–O and As–Al distances of 1.75 and 3.24 Å, respectively. EXAFS results also demonstrated As(III) complexation to three oxygen atoms in the first shell, at a distance of 1.77 Å, and to aluminum in the second shell at a distance of 3.21 Å, characteristic of bidentate–binuclear configuration, at pH 5.0, 7.0 and 9.0. Another As–Al interaction, attributed to the monodentate–binuclear complex due to its distance of 3.49 Å, was shown from EXAFS results to provide a minor contribution to As(III) sorption on gibbsite. Therefore, results from theoretical calculations and experimental measurements confirmed the occurrence of inner-sphere complexation during the As(III) adsorption on gibbsite, in a pH range of 5–9. Hence, the higher As(III) mobility in the environment, when compared to As(V), was suggested to be related to the protonation of the As(III) adsorbed complexes. This protonation would restore the neutral H_3AsO_3 molecule, which could be then released from the mineral surface. These results might be useful to predict and control arsenic mobility in aqueous environments, particularly where Al oxy-hydroxides are often found.

* Corresponding author. Address: Department of Metallurgical and Materials Engineering, Universidade Federal de Minas Gerais, Av. Antonio Carlos, 6627, Engineering School, Bloco 2, s/2233, Campus Pampulha, 31270-901, Belo Horizonte, Minas Gerais, Brazil. Fax: +55 31 34091825/1817.

E-mail address: ciminelli@demet.ufmg.br (V.S.T. Ciminelli).

0016-7037/$ - see front matter © 2011 Elsevier Ltd. All rights reserved.
doi:10.1016/j.gca.2011.12.019

1. INTRODUCTION

Arsenic immobilization on iron and aluminum oxy-hydroxides has been the subject of much investigation in the past few decades (Fendorf et al., 1997; Hering et al., 1997; Manning et al., 1998; Goldberg and Johnston, 2001; Dixit and Hering, 2003; Ladeira and Ciminelli, 2004; Kubicki, 2005). Some of these studies have reported that iron oxy-hydroxides are more efficient for arsenic removal from aqueous solutions than the analogous aluminum phases. However, the higher arsenic uptake by Fe oxy-hydroxides may be a consequence of their usually higher specific surface area and not due to a significant difference in the capacity of iron and aluminum compounds to adsorb arsenic. When the solid's specific surface area is also considered, the differences in the arsenic uptake amongst the various iron oxide and oxy-hydroxides and aluminum hydroxide are not so evident. Corroborating with this observation, Silva et al. (2010) found that, on a weight basis, the maximum As(V) uptake by various minerals followed the sequence: Ferrihydrite (1.258 ± 0.034 mmol g^{-1}) > Gibbsite (0.228 ± 0.006 mmol g^{-1}) > Hematite (0.193 ± 0.006 mmol g^{-1}) > Goethite (0.101 ± 0.002 mmol g^{-1}). On the other hand, when the specific surface area of the solids was also taken into account, all the Fe and Al oxy-hydroxides tested reached a maximum adsorption capacity of approximately 0.005 mmol m^{-2}. An additional contribution of aluminum oxy-hydroxides to arsenic fixation comes from the fact that arsenic may be released eventually to the environment due to reductive dissolution of the Fe(III) oxy-hydroxides, while the solubility of Al(III) oxy-hydroxides is not as strongly affected by redox processes (Meng et al., 2001; Masue et al., 2007; Silva et al., 2010).

Gibbsite, α-$Al(OH)_3$ (Saalfeld and Wedde, 1974), is a particularly important aluminum oxy-hydroxide commonly found in abundance in tropical soils (Macedo and Bryant, 1987; Schaefer et al., 2008), and it is known to play a significant role during arsenic natural attenuation in the environment (Ladeira and Ciminelli, 2004; Mello et al., 2006). An important example is the work done by Mello et al. (2006), in which As-enriched soils and sediments from different mining regions of Brazil were investigated. The work shows that the low values of soluble As from the evaluated samples is related to the presence of gibbsite, a large amount of iron oxides, and a lack of organic matter in the solid phase. The environmental implications of the presence of gibbsite were also highlighted, since it is thermodynamically more stable than iron oxides under anaerobic conditions, such as those found in waterlogged soils and lake sediments. In another work, Pantuzzo and Ciminelli (2010) investigated arsenic association and the long-term stability of disposed arsenic residues. The authors have found indications that, in addition to iron and calcium, arsenic was also associated to Al in the form of Al-arsenate co-precipitates in the residues aged for around 20 years. These findings corroborate our group's initial results on the main oxisol features responsible for As fixation in mining areas, which showed a good correlation between arsenic uptake and aluminum oxides content in the soil samples (Ladeira and Ciminelli, 2004). Hence, a better understanding about how arsenic species interact with aluminum hydroxides, especially gibbsite, is expected to advance the prediction and control of As distribution in aqueous environments (Arai et al., 2001; Ladeira et al, 2001; Weerasooriya et al., 2004).

Most of the previous work has focused on the As(V) species. In a convincing study, Ladeira et al. (2001) have elucidated the mechanism of As(V) immobilization on gibbsite. Results from Extended X-ray Absorption Fine Structure (EXAFS) analysis and Density Functional Theory (DFT) demonstrated that As(V) formed preferably an inner sphere bidentate–binuclear complex on the surface of Al oxy-hydroxyl octahedra at pH around 5. Regarding the trivalent arsenic species, there have been few studies focused on its immobilization on gibbsite. Weerasooriya et al. (2003) proposed that As(III) forms outer-sphere surface complexes on gibbsite surface, based on the ionic strength and pH dependences of the sorption. Ladeira and Ciminelli (2004) evaluated arsenic sorption/desorption behavior on an oxisol and its main constituents and they demonstrated a significant uptake of both As(V) and As(III) by gibbsite, respectively 4.6 mg g^{-1} and 3.3 mg g^{-1}. However, while only a maximum of 2% of the sorbed As(V) was leached from the selected samples, As(III) leaching reached up to 32% in the presence of sulfate ions. According to the authors, the formation of outer-sphere complexes would explain the relatively higher remobilization observed for As(III), compared to As(V) species. However, the authors affirmed that their preliminary spectroscopic data obtained for As(III) loaded onto natural gibbsite pointed to the existence of inner-sphere neutral complexes at pH 5.5. Some studies on As(III) immobilization onto different aluminum mineral phases have also shown divergent results. Goldberg and Johnston (2001) reported that As(III) exhibits only a weak affinity for amorphous Al_2O_3, resulting in the formation of an outer-sphere complex. In contrast, Arai et al. (2001) concluded that As(III) forms predominantly an inner-sphere bidentate binuclear complex on γ-Al_2O_3, at pH 5.5.

As can be seen from the above, there is no consensus about the mechanism of the As(III) immobilization on aluminum oxy-hydroxides. Furthermore, Ladeira and Ciminelli (2004) showed that significant amounts of As(III) were retained on different soil constituents, but around 30% of this were released during desorption tests. Thus, it is reasonable to consider that the environmental impacts caused by As(III) mobility is related to this peculiar desorption behavior rather than to a limited As(III) uptake by the minerals. Therefore, identifying a mechanism that could bring together all experimental observations is still a challenge. In a theoretical approach, Oliveira et al. (2006) used density functional methods and cluster models to study two possible processes for the As(III) immobilization on gibbsite: (i) the acid/base (ab) mechanism in which H_3AsO_3 behaves like an Arrhenius acid reacting with the base surface of gibbsite; (ii) the non-dissociative (nd) mechanism in which the H_3AsO_3 is adsorbed having the OH group bridging the As and Al atomic centers. According to the authors, this non-dissociative mechanism could reconcile the high remobilization of As(III) with the apparently inconsistent

formation of inner-sphere adsorption complexes. However, we are not aware of experimental data supporting this proposed mechanism.

Considering the aforementioned context, the present work combines DFT calculations and EXAFS analyses to elucidate the structural environment of As(III) surface complexes on gibbsite, aiming at predicting their stability in Al-rich aqueous environments and, consequently, their potential for remobilization. Various adsorption modes for As(III) linkage on the gibbsite surface were investigated by means of theoretical calculations. Fig. 1 shows the configurations assessed in the present work. The monodentate–mononuclear (mm) complex refers to the configuration in which a single oxygen atom from the arsenite oxyanion coordinates to a single structural aluminum at the Al-hydroxide surface. In a monodentate–binuclear (mb) complex, a single oxygen atom from the arsenite oxyanion is coordinated to two structural Al at the Al–OH surface; in a bidentate–mononuclear (bm) complex, two oxygen atoms from the arsenite oxyanion coordinates a single structural Al at the Al–OH surface; and, finally, in a bidentate–binuclear (bb), two oxygen atoms from the arsenite oxyanion are coordinated to two structural Al atoms at the Al–OH surface. The "ab" and "nd" designations indicate if acid–base or non-dissociative sorption mechanisms were considered. The EXAFS data were collected for As(III) immobilized on gibbsite surface at different pH values (5.0, 7.0 and 9.0) and, as a result, different coverage levels.

2. COMPUTATIONAL AND EXPERIMENTAL METHODS

2.1. Computational approach

The adsorption of H_3AsO_3 on gibbsite is particularly challenging for theoretical calculations. Previous investigation by our research group (Oliveira et al., 2006) indicates that many different adsorption sites are available on the gibbsite surface. In this work, monodentate–mononuclear (mm), monodentate–binuclear (mb), bidentate–mononuclear (bm) and bidentate–binuclear (bb) complex configurations were considered for As(III) sorption on the (0 1 0) gibbsite surface, which is representative of all ($hk0$) gibbsite edge surfaces, shown to be more reactive than the (0 0 1) basal surface (McBride and Wesselink, 1988). The surface model (see Fig. 2) was derived from the relaxed bulk structure of gibbsite. The bulk structure was relaxed by proportionally varying the cell parameters a, b, and c and performing a full relaxation of the atomic positions until the lowest energy cell was found. In this case, we have obtained $a = 9.004$ Å, $b = 5.265$ Å, and $c = 10.095$ Å, which are 3% larger than the experimental values [Saalfeld and Wedde, 1974]. To build the gibbsite (0 1 0) surface model, a periodic slab with approximately 25 Å thickness was cut parallel to the (0 1 0) plane of the relaxed gibbsite bulk, resulting in Al-terminated surfaces. Then, each one of the surface Al atoms was saturated by adding a terminal OH

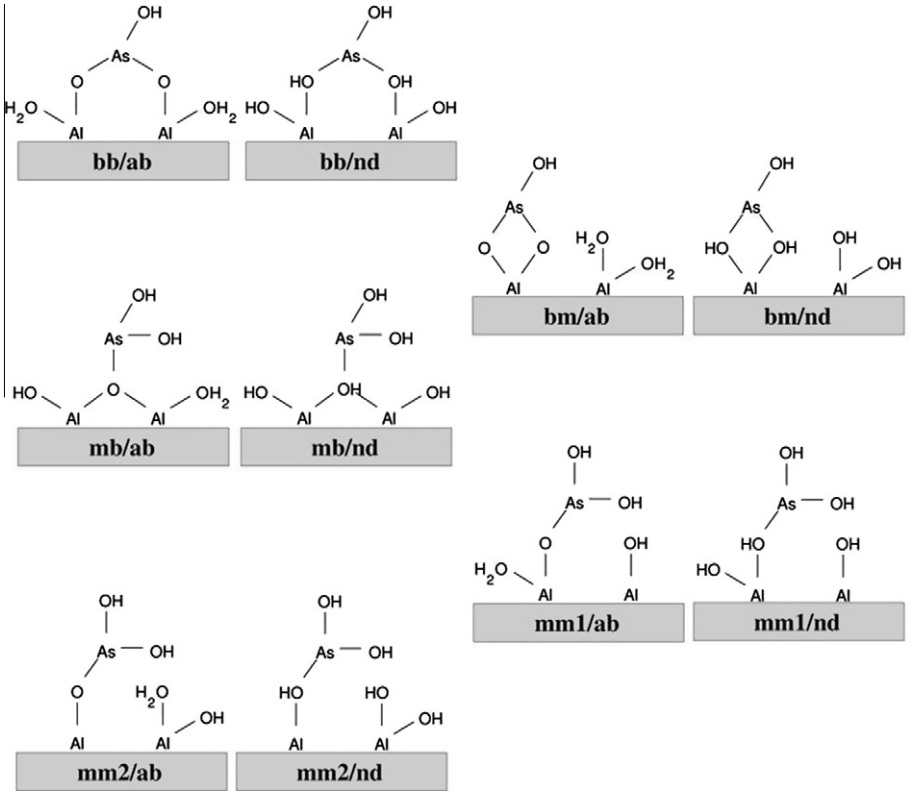

Fig. 1. Different adsorption complexes of As(III) on gibbsite investigated using the theoretical approach. Nomenclature of the sites: (mm): monodentate–mononuclear, (mb): monodentate–binuclear, (bm): bidentate–mononuclear, (bb): bidentate–binuclear. The "ab" and "nd" designations indicate if acid–base or non-dissociative sorption mechanisms were considered.

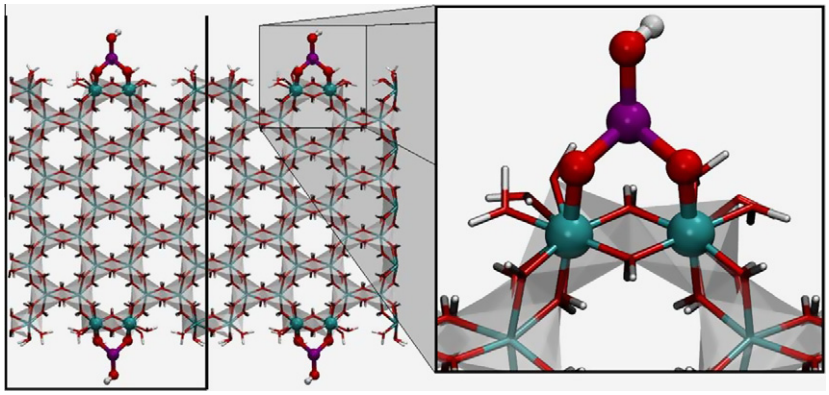

Fig. 2. Perspective view of the bb/ab adsorption complex in the edge of the gibbsite.

group and a coordinated water molecule, in order to restore the octahedral geometry of the Al atoms and neutralize the net electric charge of the model. In addition, a vacuum region of at least 100 Å was added above the slab to ensure that the model does not interact with its own periodic image along the *b* direction. Finally, the slab was replicated once along the *a* direction, to make room for the adsorbates. The final supercell of gibbsite (0 1 0) had the following dimensions: $a = 18.008$ Å, $b = 130$ Å (including the vacuum region), $c = 10.095$ Å, and $\beta = 94.54$. From this gibbsite (0 1 0) model, the adsorption complexes shown in Fig. 1 were constructed by adding one As(III) species below and above the slab, in a total of 554 atoms per model.

The potential energy surface (PES) was explored using the Born–Oppenheimer molecular dynamics (MD) prior to the geometry optimization in order to increase the probability of finding the true global minimum of the potential energy surface. The MD step consisted of linear increase of the temperature up to 320 K in 250 fs, followed by 1000 fs at constant temperature, ending with exponential temperature decrease down to 0 K in 250 fs. The geometry optimization was then performed with the conjugate-gradient algorithm until the maximum force component was lower than 10^{-4} a.u. The potential energy surface (PES) was calculated using the self-consistent charge corrected density-functional based tight-binding (SCC-DFTB) method (Elstner et al., 1998). The PES calculated using the SCC-DFTB was used for performing both MD and geometry optimizations.

The SCC-DFTB method is an approximate density functional theory (DFT) scheme which employs minimal set of atomic basis functions and tight-binding-like approximations. In the DFTB method the three center integrals are neglected and the overlap and two center integrals are previously tabulated and recorded, the so called Slater–Koster files. Then, the secular matrices are easily built, making the calculations much faster. The total energy has to be corrected due to the approximation made in the hamiltonian by introducing a repulsive potential which is fitted with respect to the DFT calculations used as reference. The self-consistent charge extension of the DFTB method allowed the distribution of charges throughout the molecular structure according to the hardness of the atoms present in the structure. The SCC-DFTB Slater–Koster files used in the present work have been developed in our laboratory (Frenzel et al., 2005) and are available in the deMon-Nano code (Heine et al., 2010), as well as in the DFTB.org website (DFTB, 2010). A recent review of the method can be found elsewhere (Oliveira et al., 2009). The SCC-DFTB has been used successfully to describe gibbsite and aluminosilicate nanotubes (Frenzel et al., 2005; Guimarães et al., 2007a). The differences between the SCC-DFTB and DFT calculated structural parameters are not larger than 0.02 Å for Al–Al and Al–O distances. When compared the SCC-DFTB calculated values with the experiment, the differences are not larger than 0.05 Å (Frenzel et al., 2005).

The Γ-point approximation was used for the geometry optimization procedures, while a set of suitable *k* points was used to sample the irreducible Brillouin zone (IBZ) during the calculation of the final total energies. The *k*-points were obtained with the Monkhorst–Pack procedure (Monkhorst and Pack, 1976; Pack and Monkhorst, 1977) and a grid of $1 \times 1 \times 2$ *k* points was determined to be enough for the calculation of total energies and assure a convergence within 10^{-3} a.u. All calculations were performed using the DFTB-plus code (Aradi et al., 2007).

2.2. Experimental approach

2.2.1. Materials

Stock arsenite solution was prepared by dissolving sodium meta-arsenite ($NaAsO_2$ at 99.99% purity – Fluka) in 18 MΩ cm Milli-Q water. Synthetic gibbsite was obtained in accordance to Silva et al. (2007), who followed the method proposed by Kyle et al. (1975). Other reagents (analytical grade) used in the experiments included sodium arsenate ($Na_2HAsO_4{\cdot}7H_2O$ at 99% purity – FLUKA), hydrochloric acid (VETEC), and sodium hydroxide (VETEC).

2.2.2. Sorption tests

Sorption tests were carried out batchwise, where 0.3 g of synthetic gibbsite was contacted with 100 mL of As(III) solution (pH 7.0 and initial concentration varying from 0 to 6.5 mmol L^{-1}) into 250 mL Pyrex Erlenmeyer flasks. The vessels were sealed with laboratory parafilm (Pechiney plastic packaging, USA) and stirred at 200 rpm and

25 ± 0.5 °C using a thermostatic shaker (New Brunswick Scientific Edison, USA). The pH was monitored and if necessary it was adjusted by adding 0.01 mol L^{-1} HCl or NaOH solutions. Ionic strength was fixed at 0.1 by adding NaCl (0.1 mol L^{-1}). After 72 h, the samples were vacuum-filtered through a 0.45 μm membrane filter (Fisher Scientific). The filtrate was analyzed for total arsenic by flame Atomic Absorption Spectroscopy, AAS (Perkin–Elmer Analyst A300). The filtered solids were rinsed with 50 mL of Milli-Q water, wet-stored in micro-centrifuge tubes (Flex-Tubes®, Eppendorf), and subsequently submitted to spectroscopic analyses. The washing step was performed to remove the remaining arsenic solution, which possibly was held in the solid phase during the sorption test. To control this step, a quantification of arsenic in the washing water was performed during the experiments. The specific surface area of the synthetic gibbsite was determined by means of BET analyses (Quantachrome Instruments, model NOVA 1000) to be equal to 45.6 $m^2 g^{-1}$. To verify if the sorption mechanism changes with pH, the loading test for the highest initial concentration was repeated at pH 5.0 and 9.0. All the sorption tests were carried out in duplicate.

2.2.3. XAFS analyses

X-ray absorption near edge structure (XANES) and extended X-ray absorption fine structure (EXAFS) analyses of the gibbsite samples loaded with As(III) were performed using the synchrotron facilities at the *Laboratório Nacional de Luz Síncrotron* (LNLS), in Campinas, Brazil. XANES and EXAFS data of the arsenic K edge (11868 eV) were obtained at XAFS2 workstation in the fluorescence mode, under operation conditions of 1.37 GeV and beam currents of approximately 250 mA. The spectra were collected at room temperature using a Si (1 1 1) double crystal monochromator with an upstream vertical aperture of 0.3 mm and calibrated with Au L_1-edge (11918 eV). The samples were fixed onto acrylic holders, sealed with Kapton tape film, placed at an angle of 40° to the incident beam, and the signal was monitored using a 15-element Ge detector (Canberra Industries). Energy calibration was monitored during data collection by acquiring reference Au foil spectra simultaneously. The obtained data were analyzed as described in Vasconcelos et al. (2008) by using the Athena and Artemis software from the IFEFFIT computer package (Ravel and Newville, 2005). Firstly, the data were processed in Athena, where several scans from the same sample were aligned by the reference spectra and merged in energy space. Edge energy value, E_0, was chosen at the inflection point of the absorption edge. Next, the pre-edge and post-edge backgrounds were removed and the spectra normalized to a step height of 1. The isolated EXAFS oscillations were converted from energy ($\chi(E)$ data) to wavenumber space ($\chi(k)$ data) and Fourier Transformed. The Fourier-transformed data were fitted using the Artemis software. Theoretical phase shift and scattering amplitude parameters were calculated by means of FEFF 6.0 code included in the IFFEFIT package (Ravel and Newville, 2005). Fits to all samples were performed using a simultaneous k-weighting of 1, 2 and 3 to decrease the possibility that correlations between fitting parameters could compensate for a misfit in a particular k-weighting. The passive electron reduction factor (S_0^2) obtained from fit to a crystalline standard (As_2O_3) was 0.95 ± 0.08 for the As K-edge. This value was used in all fits to the data.

3. RESULTS

3.1. SCC-DFTB calculations of As(III) adsorption on gibbsite

Different adsorption sites were investigated using the slab model of the surface as shown in Fig. 1. In order to allow a direct comparison of the different adsorption complexes, H_2O or –OH groups were added to keep their charge neutrality and the coordination number of the Al centers. The results for the most favorable adsorption sites are shown in Table 1. All the other adsorption sites are at least 50 kcal mol^{-1} higher in energy and will not be discussed here.

Regarding the solvent effects, there is a consensus in the literature (Kubicki et al., 2007; Hatorri et al., 2009) that placing water molecules in the empty coordination sites of the metal centers is crucial to permit a reasonable description of the thermodynamics of the system and, consequently, the chemical speciation. Indeed, it has been the subject of many studies (Abreu et al., 2006,2008; Guimarães et al., 2007b; Noronha et al., 2007; Rodrigues et al., 2011). However, in the case of the arsenous acid, at the pH range used at the experiments, the predominant species is fully protonated H_3AsO_3, (pKa ~9). The process of adsorption may thus follow the two mechanisms suggested by Oliveira et al. (2006). It can be asked if water molecules surrounding the H_3AsO_3 forming hydrogen bonds are not necessary. In Oliveira et al. (2006) this possibility is discussed in detail. In summary, it is reasonable to expect that the solvation energy of the surface occupied by the H_3AsO_3 is similar to the solvation energy of the H_3AsO_3 itself, leading to a cancelation of errors. Furthermore, the present study is more interested in obtaining accurate geometries and relative energies of the different adsorption sites, and the solvent effects do not seem to change drastically the relative stability of the complexes evaluated in this work.

The structural parameters are known to be a local property, therefore the model used is adequate and reliable. The most difficult part is to assure that the potential energy surface has been explored enough to find the most favorable adsorption site. Using the approximate DFT method, larger models can be used to investigate a larger number of

Table 1
Relative energies and structural parameters of the most favorable adsorption complexes.

Adsorption site	ΔE (kcal mol^{-1})	As–Al distance (Å)	As–O distance (Å)
bb/ab	0.0	3.24	1.75
mm/ab	11.2	3.27	1.67
mm/nd	33.3	3.38	1.66
bb/nd	51.0	3.03	1.81
mb/ab	90.5	3.46	1.79

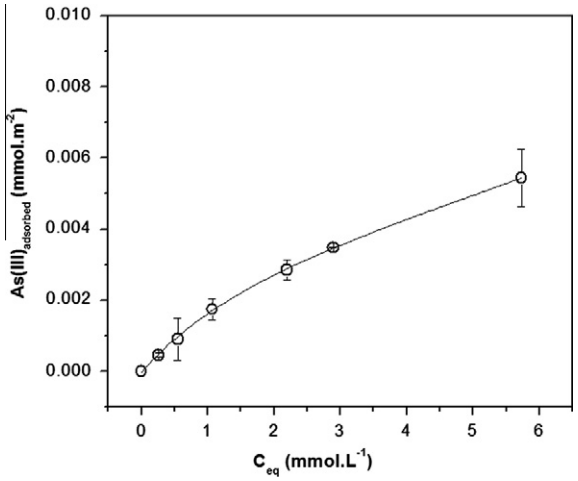

Fig. 3. Isotherm for As(III) adsorption on gibbsite at pH 7.0, 25 °C, 200 rpm, ionic strength of 0.1, and S/L ratio of 3 g L^{-1}. Sorption tests were carried out in duplicates.

possible sites, thus making the method particularly interesting to the present investigation. Therefore, the molecular dynamic simulation has been used together with the SCC-DFTB to explore the vicinities of each adsorption mode described in Fig.1. The binuclear–bidentate/acid–base adsorption (bb/ab) shown in Fig. 2 was found to be the most stable complex for As(III) adsorption on gibbsite surface with As–Al and As–O distances of 3.24 and 1.75 Å, respectively. These values are in good agreement with the DFT calculations on small cluster models performed by Oliveira et al. (2006), who obtained 3.21 Å for the As–Al distance in the bb/ab adsorption complex.

3.2. XAFS analyses of As(III) adsorption on gibbsite

Fig. 3 shows the isotherm obtained for As(III) sorption on gibbsite (BET specific surface area of 45.6 m^2 g^{-1}) at pH 7.0, where the highest coverage level was found to be equal to 0.0054 $mmol_{As(III)}$ m^{-2}. This sorption experiment was repeated at pH 5 and 9, and it was found that the loading was lower at pH 5.0 (0.0025 $mmol_{As(III)}$ m^{-2}) than at pH 7. At pH 9.0 the loading was equal to 0.0058 $mmol_{As(III)}$ m^{-2}, which is similar to the value found at pH 7. The samples used for XAFS analyses in the present work are summarized in Table 2. XAFS measurements were also carried out with lower As(III) surface coverage levels and they are presented in the electronic annex (EA). The results for the samples near the surface saturation conditions for each pH were further explored as they combine two features of interest: (i) the different sorption capacities at each pH, and (ii) the potential effects of pH on the sorption mechanisms.

Table 2
List of samples used for XAFS analyses.

Samples	pH	$[As]_{adsorbed}$ (mmol m^{-2})
I	5.0	0.0025
II	7.0	0.0054
III	9.0	0.0058

Fig. 4(a) compares the normalized As K-edge XANES spectra of evaluated samples and standards. Fig. 4 (b), (c) and (d) show the derivative As K-edge XANES spectra for the As(III)–Gibbsite sorbed at pH 9.0, 7.0, and 5.0, respectively, compared to the solution and solids standards. As can be seen, the derivative spectra for the As(III)-Gibbsite samples overlaps the derivative spectra of the $NaAsO_2$ standard at all pH assessed. This indicates that As(III) was not oxidized, at least not significantly, to As(V) during the sorption process. The possibility of As(III) oxidation by the beamline was also checked and it was not verified the occurrence of such process.

To investigate the local structure of arsenic on gibbsite, the Fourier-transformed EXAFS spectrum was fitted using As–O and As–Al scattering paths derived from the structures of sodium meta-arsenite ($NaAsO_2$), mansfieldite ($AlAsO_4{\cdot}2H_2O$) and Al-substituted tooeleite ($Al_6(AsO_3)_4SO_4(OH)_4{\cdot}4H_2O$). These paths were obtained from the built-in FEFF 6.0 code of the Artemis software (Ravel and Newville, 2005). The three datasets assessed were fit simultaneously (R range from 1.0 to 3.5 Å) with a single ΔE_0 value. This method is useful when a similar model is applied to fit a series of samples. Besides, fitting datasets simultaneously increases the number of independent data points, which decreases errors associated with the fitting parameters and decreases correlations between variables, increasing then the confidence in the final fitted values. During the fitting, the coordination number (N) for the As–Al interaction was set at 1 or 2, which designate different fit models. The fit with the N set at 1 considered the occurrence of mm or bm complex types, where a single or two oxygen atoms from the arsenite oxyanion are coordinated to a single aluminum at the Al-hydroxide surface. The N set at 2 could indicate the occurrence of bb or mb complex configurations, in which a single or two oxygen atoms from the arsenite oxyanion, respectively, are coordinated to two Al at the Al–OH surface.

Fig. 5(a) shows the real part of the Fourier-transformed EXAFS region of the As K-edge XAFS spectra for the gibbsite loaded with As(III) at different pH values, together with the best fitting curve for each sample. The individual contributions of the As–O, and As–Al scattering paths to the fits of the sample at pH 7.0 are shown in Fig. 5(b). Due to similarities with the pH 7 sample, the other two samples (pH 5 and 9) are not repeated in Fig. 5(b). However, they were fitted using the same scattering paths shown for pH 7. EXAFS oscillations (multiplied by k^3 to enhance features at high k values) of the samples and their respective fits to the data are shown in Fig. 5 (c). All data were Fourier transformed in the range $k = 3.2$ Å^{-1} to $k = 12$ Å^{-1}. Fig. 5(d) shows the magnitude EXAFS spectra of the samples at the evaluated pH. The best fits to EXAFS data are summarized in Table 3. During the fitting, the number of independent points and variables were equal to 41.5 and 22, respectively. The relative misfit (R-factor) was around 1% for all tested configurations. The χ^2-reduced factor is shown in Table 3 for each fitting configuration.

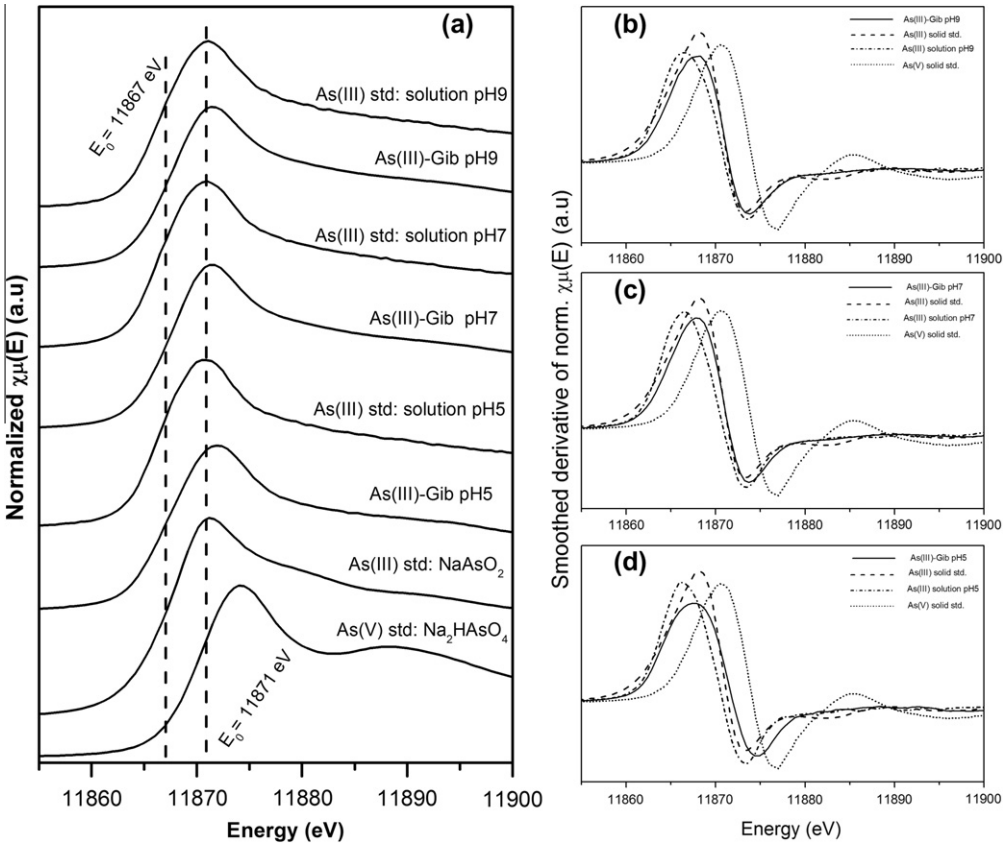

Fig. 4. (a) Normalized As K-edge XANES spectra of As(III)-loaded gibbsite, As(III) solutions at pH 5.0, 7.0, and 9.0; and $NaAsO_2$ and $Na_2HAsO_4{\cdot}7H_2O$ solid standards; (b) (c) and (d): Smoothed derivative of the normalized As K-edge XANES spectra for As(III)-loaded gibbsite and As(III) solution at pH 9.0, 7.0, and 5.0, respectively, besides $NaAsO_2$ and $Na_2HAsO_4{\cdot}7H_2O$ solid standards.

Results shown in Table 3 indicate that at pH 7.0 the arsenic atom is coordinated by 3.3 ± 0.2 oxygen atoms at a distance of 1.77 ± 0.01 Å in the first shell. The coordination number of 3 oxygen atoms in the first coordination shell is in agreement with the expected pyramidal geometry of the As(III) species, H_3AsO_3, predominant in solution at pH <9.0. Regarding the second shell, firstly only the As–Al_1 path (from mansfieldite structure) contribution to the fitting was considered, with coordination number (N) set at 1 or 2. At pH 7.0, the fitting returned an As–Al_1 distance of 3.20 ± 0.03 Å for $N = 2$, and an As–Al_1 distance of 3.18 ± 0.03 for $N = 1$. Thus, it is reasonable to say that the As–Al distances are very similar (around 3.2 Å), independent of the coordination number considered in the fitting. This observation gives the confidence that the As–Al distance in the second shell is in fact around 3.2 Å. It is known from literature that the typical interatomic distance for As–Al and As–Fe interactions when arsenic is sorbed on Al and Fe oxy-hydroxides at bidentate–binuclear configuration is approximately 3.2 Å (Arai et al., 2001; Ladeira et al., 2001; Sherman and Randall, 2003). Therefore, the As–Al distance from our EXAFS results is in agreement with the literature, indicating the occurrence of bidentate–binuclear complexation of As(III) on gibbsite at the conditions evaluated in the present work.

With respect to the more dilute samples (see electronic annex), it was found that at pH 7.0 the As(III) is coordinated to 3.1 ± 0.3 oxygen atoms at a distance of 1.77 ± 0.01 Å in the first shell; to aluminum at a distance of 3.23 ± 0.06 Å, and to another Al atom at a distance of 3.5 ± 0.1 Å. The number of independent points and variables in this case were 55.4 and 29, respectively (χ^2-reduced = 43.9 and R-factor = 1%).

Regarding the pH effects on the As(III) complexation on gibbsite, the As–O and As–Al interatomic distances remained virtually unchanged regardless of the value of pH evaluated (Table 3). This suggests that, although the As(III) loading increases with increasing pH from 5 to 9, its preferable sorption mechanism on gibbsite was not significantly dependent on the pH, under the conditions of the present investigation.

During the fitting to EXAFS data, the contribution of another As–Al interaction in the system became apparent, and thus an As–Al_2 path (from Al-substituted tooeleite structure) was added to the model. The As–Al_2 path was considered using different coordination numbers (set at 1 and 2), and all of them have returned similar As–Al interatomic distances (~3.49 Å). By comparing the As–Al experimental distance (3.47 ± 0.04 Å) to the results from theoretical calculations shown in Table 1, it is possible to verify that the value is close to the monodentate–binuclear (mb) configuration. To elucidate the improvement in the fit to the data when considering a second As–Al path in the model, the fit in the range 2.3–3.5 Å was carried out in

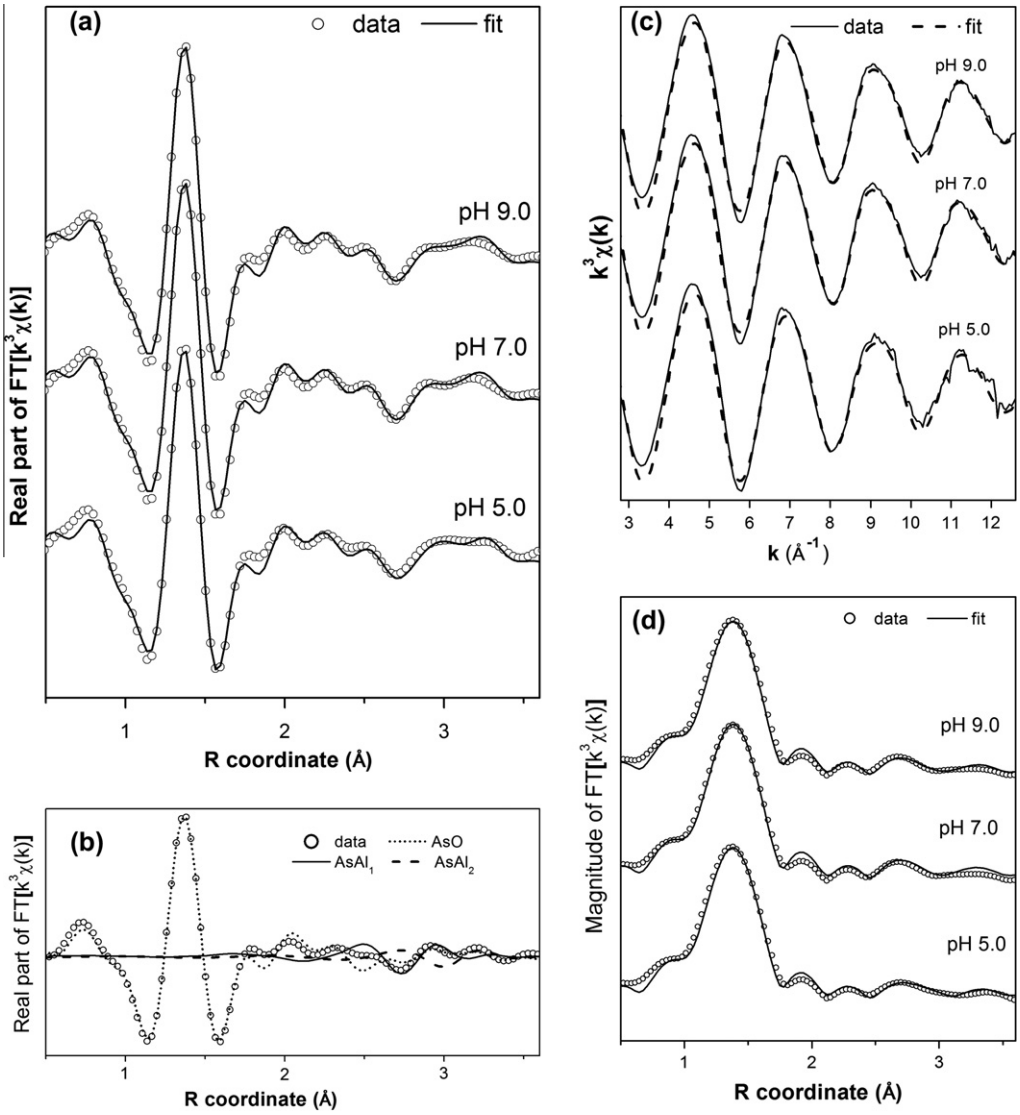

Fig. 5. (a) Real part of the Fourier-transformed As K-edge EXAFS data for (a) As(III)-loaded gibbsite at different pH values – scatter and line curves represent data and fit, respectively; (b) individual contributions of scattering paths used to the fits; (c) k^3-weighted $\chi(k)$ data (solid line) and their respective fit (dashed line) for As(III) on gibbsite at different pH values; and (d) magnitude of the Fourier-transformed As K-edge EXAFS data for As(III)-loaded gibbsite at different pH values.

the presence and absence of this As–Al_2 path. As can be seen in Fig. 6, the addition of the As–Al_2 path in the model improves the fit. In fact, the χ^2-reduced factor decreased from 35 to 24 and the relative misfit (*R*-factor) decreases from 12% to 5% in the range of 2.3–3.5 Å.

4. DISCUSSION

Comparing the theoretical and experimental results, it is observed a convergence between the optimized geometry and the obtained geometrical EXAFS parameters. SCC-DFTB calculations indicated the bidentate–binuclear complex (bb/ab) to be the most favorable geometry for As(III) linkage on gibbsite surface with As–O and As–Al distances of 1.75 and 3.24 Å, respectively. EXAFS results found that arsenic is coordinated to 3 oxygen atoms at a distance of 1.77 Å in the first shell, and bonded to aluminum at a distance around 3.2 Å regardless of the coordination number considered for the second shell (1 or 2) and the pH assessed (5, 7 and 9). This As–Al distance of 3.2 Å is found in the literature to be typical of inner-sphere bidentate–binuclear complexation of arsenic on Al and Fe oxides and oxyhydroxides (Arai et al., 2001; Ladeira et al., 2001; Sherman and Randall, 2003). Thus, EXAFS results and theoretical estimates provide evidences that, amongst the evaluated geometries, inner-sphere bidentate binuclear complexation is the preferable configuration for the As(III) on gibbsite surface. It is important to highlight that the fits to EXAFS data were not based on DFT results, and that these modeling techniques were performed in a completely independent manner. The good agreement between these independent approaches supports the conclusions of the present work.

Table 3
Results of fits to EXAFS data.

Samples	As–O			As–Al_1			As–Al_2			ΔE_0 (eV)	$\chi^2_{Red.}$
	N	R (Å)	σ^2 (Å^2)	N^a	R (Å)	σ^2 (Å^2)	N^a	R (Å)	σ^2 (Å^2)		
I (pH 5)	3.4 ± 0.2	1.771 ± 0.004	0.005 ± 0.001	2	3.21 ± 0.03	0.011 ± 0.005	2	3.49 ± 0.06	0.019 ± 0.011	11.1 ± 0.7	54.2
							1	3.49 ± 0.07	0.011 ± 0.009	11.1 ± 0.7	57.4
				1	3.18 ± 0.04	0.006 ± 0.004	2	3.43 ± 0.07	0.023 ± 0.015	11.0 ± 0.7	57.8
							1	3.43 ± 0.09	0.014 ± 0.014	10.9 ± 0.8	62.5
II (pH 7)	3.4 ± 0.2	1.773 ± 0.004	0.004 ± 0.001	2	3.20 ± 0.03	0.010 ± 0.004	2	3.47 ± 0.04	0.014 ± 0.006	11.1 ± 0.7	54.2
							1	3.47 ± 0.04	0.007 ± 0.005	11.1 ± 0.7	57.4
				1	3.18 ± 0.03	0.005 ± 0.003	2	3.43 ± 0.06	0.019 ± 0.009	11.0 ± 0.7	57.8
							1	3.42 ± 0.06	0.010 ± 0.008	10.9 ± 0.8	62.5
III (pH 9)	3.4 ± 0.2	1.773 ± 0.004	0.005 ± 0.001	2	3.20 ± 0.03	0.011 ± 0.004	2	3.47 ± 0.05	0.016 ± 0.007	11.1 ± 0.7	54.2
							1	3.47 ± 0.05	0.008 ± 0.005	11.1 ± 0.7	57.4
				1	3.18 ± 0.03	0.006 ± 0.004	2	3.42 ± 0.06	0.019 ± 0.010	11.0 ± 0.7	57.8
							1	3.42 ± 0.06	0.011 ± 0.008	10.9 ± 0.8	62.5

R = Interatomic distance; N = coordination number; σ^2 = Debye–Waller factor; ΔE_0 = difference between the user-defined and the experimentally determined threshold energy; $\chi^2_{Red.}$: chi-square reduced; number of independent points = 41.5; number of variables = 22; relative misfit (R-factor) = 1% (all fitting configurations).
[a] Fixed parameter.

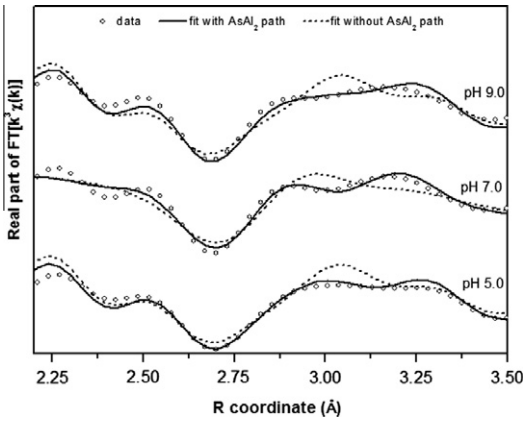

Fig. 6. Real part of the Fourier-transformed As K-edge EXAFS data in the range 2.3–3.5 Å for As(III)-loaded gibbsite at different pH values. Scatter and line curves represent data and fit, respectively.

One may argue about the method used to fit the EXAFS data by setting an important parameter as the coordination number (N). It is important to make clear that the authors are aware of the limitations of such an approach. However, the proposition of the inner-sphere bidentate–binuclear complexation as the preferable configuration for the evaluated system has been based on the observed interatomic As–Al distance, and not in the coordination number, which was fixed for the second shell during the fit. Furthermore, considering that the system under study in this work is not a well-ordered one, and the quality of the data is unavoidably limited by operating conditions, it is suitable to use the alternative of setting parameters to reach an accurate fitting. Indeed, this approach of constraining some parameters during EXAFS fitting is usually found in the literature (Arai et al., 2001,2004; Bostick and Fendorf, 2003; Sherman and Randall, 2003; Paktunc et al., 2008; Chen et al., 2009; Voegelin et al., 2010). Some of these mentioned investigations have set the coordination numbers (Bostick and Fendorf, 2003; Paktunc et al., 2008; Chen et al., 2009; Voegelin et al., 2010) while others have fixed the Debye–Waller factor (Arai et al., 2001,2004; Sherman and Randall, 2003) for the second shell fitting. In this work, it was chosen to set the coordination number instead of the Debye–Waller factor because of previous indication from theoretical calculations regarding the possible coordination numbers for the As(III)-gibbsite system. As shown in Section 3.1, the most thermodynamically favorable configurations for the As–Al interaction would present coordination numbers of 2 or 1. These values are also supported by the results obtained in similar systems (Arai et al., 2001; Ladeira et al., 2001; Sherman and Randall, 2003).

Regarding the contribution of the As–Al_2 interaction in the system, the improvement in the fitting quality was evidenced when considering this path in the model (Fig. 6). One may argue about the relatively high energy of the mb/ab sorption complex used to fit the As–Al_2 contribution in the EXAFS spectra, when compared to the other configurations evaluated during theoretical calculations. However, larger distances generally mean weakly bound

complexes, as suggested by the mb/ab-calculated As–Al distance of 3.47 Å. Therefore, other effects such as ionic strength, pH and solvation might be important to be considered in order to accurately simulate the thermodynamics (e.g. energy) of the system. The relative stability of the different adsorption sites may be easily modified upon consideration of these effects. However, the geometry (e.g. distances) of these sites is not expected to be significantly altered by these effects, since adsorption is a local phenomenon. The EXAFS estimated As–Al_2 distance of 3.49 Å is in good agreement with the mb/ab adsorption site as shown in Table 3, and the As–O distance of 1.77 Å is about 0.03 Å lower than the calculated value. These results indicate that the mb/ab adsorption site may be assigned as the adsorption site observed in the As–Al_2 path proposed in the EXAFS analyses, despite its relatively high energy.

Considering the literature regarding As(III) interactions on gibbsite, Weerasooriya et al. (2003) proposed that As(III) forms an outer-sphere surface complex with gibbsite. These authors based their suggestion on indirect macroscopic evidences of sorption dependency with pH and ionic strength. Goldberg and Johnston (2001) also suggested that As(III) forms outer-sphere complexes on amorphous $Al(OH)_3$ considering their results from Raman and FTIR spectroscopy, sorption, and electrophoretic mobility measurements. Arai et al. (2001) used XAFS analyses to propose a mechanism for As(III) sorption on alumina (γ-Al_2O_3) at pH 5.5 and 8.0. The results for As–O (1.75–1.78 Å) and As–Al (3.19–3.22 Å) interatomic distances are similar to the As–O (1.77 Å) and As–Al_1 (3.21 Å) values obtained in the present work. These authors suggested that As(III) forms a bidentate–binuclear complex on alumina surface at pH 5.5, regardless of the ionic strength (*IS*). At pH 8.0, a mixture of inner- and outer-sphere As(III) complexes would coexist, with outer-sphere complexes becoming more important as ionic strength decreases. These authors based their hypothesis of a change in the sorption mechanism on XANES analyses. According to them, the spectrum of the sample reacted at pH 8 and $IS = 0.01$ mol L^{-1} appeared to be intermediate between the aqueous As(III) spectrum and the spectra of the other As(III) adsorption samples. It was then suggested that this apparent difference indicated a mixture of inner-sphere and outer-sphere As(III) complexes at pH 8. In the present work, no significant alterations in XANES spectra of As(III) immobilized on gibbsite were found as pH increased from 5 to 9 (see Fig. 4).

In summary, the present work demonstrates the formation of inner-sphere bidentate–binuclear complexes during As(III) sorption on gibbsite surface according to both theoretical and experimental techniques. It should be clarified that the formation of outer-sphere complexes cannot be disregarded. However, it is clear from our DFT and EXAFS results that inner-sphere complexation of As(III) occurs on gibbsite, a fact that has not been widely recognized yet in the literature.

Regarding the practical implications of the results obtained in the present work, one may consider the often-stated argument that the As(III) mobility in the environment is higher than the As(V) mobility due to the neutral character of the arsenite molecule in a wide pH range (<9.2) as too simplistic. Like As(V) (Ladeira et al., 2001), As(III) was also demonstrated to form inner-sphere complexes on gibbsite's surface in a pH interval (pH 5–9) where the neutral H_3AsO_3 predominates. In order to understand such higher mobility of the As(III) it is important to notice the following: the first pK_a of H_3AsO_3 is about 9.2, and the point of zero charge (pzc) of gibbsite and other aluminum oxides is in the pH range of 8–10 (Arai et al., 2001; Goldberg and Johnston, 2001; Ladeira and Ciminelli, 2004). It means that the gibbsite surface has similar ability to accept protons as the As(III) sorbed complex. Therefore, it is proposed that the higher As(III) mobility in the environment is related to the of protonation of the inner-sphere As(III) complexes, in addition to the protonation of the Al oxyhydroxides surfaces. The protonation would restore the neutral H_3AsO_3 molecule, which would then be released from the mineral surface.

5. CONCLUSIONS

The results from theoretical calculations combined with EXAFS analyses obtained in this work indicate that inner-sphere complexation is a feasible mechanism for arsenite adsorption on gibbsite at pH varying from 5 to 9. Several adsorption sites have been evaluated using SCC-DFTB calculations and the most stable structure predicted for the As(III)-gibbsite system is the bidentate–binuclear configuration. EXAFS results also indicated that As(III) forms inner-sphere complexes on gibbsite. It was shown that the arsenic coordinated to three oxygen atoms in the first shell, at a distance of 1.77 Å, and to aluminum in the second shell at a distance of approximately 3.20 Å, typical of bidentate–binuclear configuration, for all evaluated pH values (5.0, 7.0 and 9.0). In addition, an As–Al_2 interaction, ascribed to the monodentate–binuclear complex because of its interatomic distance of 3.47 Å, was shown from EXAFS results to contribute to As(III) sorption on gibbsite, considering the conditions used in this work. Based on these results, it was proposed that the higher As(III) mobility in the environment, when compared to As(V), may be related to the protonation of the As(III) inner-sphere complexes formed on the mineral surface. Such protonation would restore the neutral H_3AsO_3 molecule, which could be easily released to aqueous environments. The understanding of As(III) interactions with gibbsite is pointed out as an important outcome from this work, considering the relevance in predicting and controlling arsenic mobility in natural environments, where gibbsite is often found.

ACKNOWLEDGMENTS

The authors would like to acknowledge the INCT-Acqua and the Brazilian agencies CNPq, Capes, and FAPEMIG. The authors express their gratitude to Dr. Johannes Frenzel, at the Ruhr-Universität Bochum – Germany, for generating the SCC-DFTB parameter files used to calculate the interatomic interactions of arsenic with Al, O and H; and to Dr. Juscimar Silva and Dr. Jaime Mello, at the Universidade Federal de Viçosa – Brazil, for supplying the synthetic gibbsite. Thanks are also extended to the National Synchrotron Light Laboratory (LNLS), Campinas, Brazil,

especially to the staff of the XAFS-2 beam line for all the support during XAFS measurements.

APPENDIX A. SUPPLEMENTARY DATA

Supplementary data associated with this article can be found, in the online version, at doi:10.1016/j.gca.2011.12.019.

REFERENCES

Abreu H. A., Guimarães L. and Duarte H. A. (2006) Density-functional theory study of iron(III) hydrolysis in aqueous solution. *J. Phys. Chem. A* **110**(24), 7713–7718.

Abreu H. A., Guimarães L. and Duarte H. A. (2008) DFT/PCM investigation of the Mn(II) chemical speciation in aqueous solution. *Int. J. Quantum Chem.* **108**, 2467–2475.

Aradi B., Hourahine B. and Frauenheim T. (2007) DFTB+, a Sparse matrix-based implementation of the DFTB method. *J. Phys. Chem. A* **111**, 5678–5684.

Arai Y., Elzinga E. and Sparks D. L. (2001) X-ray absorption spectroscopic investigation of arsenite and arsenate adsorption at the aluminum oxide–water interface. *J. Colloid Interface Sci.* **235**, 80–88.

Arai Y., Sparks D. L. and Davis J. A. (2004) Effects of dissolved carbonate on arsenate adsorption and surface speciation at the hematite–water interface. *Environ. Sci. Technol.* **38**(3), 817–824.

Bostick B. C. and Fendorf S. (2003) Arsenite sorption on troilite (FeS) and pyrite (FeS_2). *Geochim. Cosmochim. Acta* **67**(5), 909–921.

Chen N., Jiang D. T., Cutler J., Kotzer T., Jia Y. F., Demopoulos G. P. and Rowson J. W. (2009) Structural characterization of poorly-crystalline scorodite, iron(III)–arsenate co-precipitates and uranium mill neutralized raffinate solids using X-ray absorption fine structure spectroscopy. *Geochim. Cosmochim. Acta* **73**, 3260–3276.

DFTB, 2010. <http://www.dftb.org> (accessed: August 12th).

Dixit S. and Hering J. G. (2003) Comparison of arsenic(V) and arsenic(III) sorption onto iron oxide minerals: implications for arsenic mobility. *Environ. Sci. Technol.* **37**, 4182–4189.

Elstner M., Porezag D., Jungnickel G., Elsner J., Haugk M., Frauenheim T., Suhai S. and Seifert G. (1998) Self-consistent-charge density-functional tight-binding method for simulations of complex materials properties. *Phys. Rev. B* **58**, 7260–7268.

Fendorf S., Eick M. J., Grossl P. and Sparks D. L. (1997) Arsenate and chromate retention mechanisms on goethite. 1. Surface structure. *Environ. Sci. Technol.* **31**(2), 315–320.

Frenzel J., Oliveira A. F., Duarte H. A., Heine T. and Seifert G. (2005) Structural and electronic properties of bulk gibbsite and gibbsite surfaces. *Z. Anorg. Allg. Chem. (ZAAC)* **631**, 1267–1271.

Goldberg S. and Johnston C. T. (2001) Mechanisms of arsenic adsorption on amorphous oxides evaluated using macroscopic measurements, vibrational spectroscopy, and surface complexation modeling. *J. Colloid Interface Sci.* **234**, 204–216.

Guimarães L., Enyashin A. N., Frenzel J., Heine T., Duarte H. A. and Seifert G. (2007a) Imogolite nanotubes: stability, electronic and mechanical propertie. *ACS Nano* **1**, 362–368.

Guimarães L., Abreu H. A. and Duarte H. A. (2007b) Fe(II) hydrolysis in aqueous solution: a DFT study. *Chem. Phys.* **333**, 10–17.

Hattori T., Saito T., Ishida K., Scheinost A. C., Tsuneda T., Nagasaki S. and Tanaka S. (2009) The structure of monomeric and dimeric uranyl adsorption complexes on gibbsite: a combined DFT and EXAFS study. *Geochim. Cosmochim. Acta* **73**, 5975–5988.

Heine T., Rapacioli M., Patchkovskii S., Frenzel J., Koester A. M., Calaminici P., Escalante S., Duarte H. A., Flores R., Geudtner G., Goursot A., Reveles J. U., Vela A., Salahub D. R. (2010). <http://www.demon-software.com/public_html/index.html>. (accessed: August, 08th).

Hering J. G., Chen P. Y., Wilkie J. A. and Elimelech M. (1997) Arsenic removal from drinking water during coagulation. *J. Environ. Eng.* **123**, 800–807.

Kubicki J. D. (2005). Comparison of As (III) and As (V) complexation onto Al and Fe-hydroxides. In Advances in Arsenic Research: Integration of Experimental and Observational Studies and Implications for Mitigation (eds. P. O'Day, D. Vlassopoulos and L. Benning). ACS Symposium Series, 915, 104–117, Washington DC.

Kubicki J. D., Kwon K. D., Paul K. W. and Sparks D. L. (2007) Surface complex structures modeled with quantum chemical calculations: carbonate, phosphate, sulphate, arsenate and arsenite. *Eur. J. Soil Sci.* **58**, 932–944.

Kyle J. H., Posner A. M. and Quirk J. P. (1975) Kinetics of isotopic exchange of phosphate adsorbed on gibbsite. *J. Soil Sci.* **26**, 34–43.

Ladeira A. C. Q. and Ciminelli V. S. T. (2004) Adsorption and desorption of arsenic on an oxisol and its constituents. *Water Res.* **38**, 2087–2094.

Ladeira A. C. Q., Ciminelli V. S. T., Duarte H. A., Alves M. C. M. and Ramos A. Y. (2001) Mechanism of anion retention from EXAFS and density functional calculations: arsenic (V) adsorbed on gibbsite. *Geochim. Cosmochim. Acta* **65**, 1211–1217.

Macedo J. and Bryant R. B. (1987) Morphology, mineralogy, and genesis of a hydrosequence of oxisols in Brazil. *Soil Sci. Soc. Am. J.* **51**, 690–698.

Manning B. A., Fendorf M. and Goldberg S. (1998) Surface structures and stability of arsenic(III) on goethite: spectroscopic evidence for innersphere complexes. *Environ. Sci. Technol.* **32**, 2383–2388.

Masue Y., Loeppert R. H. and Kramer T. A. (2007) Arsenate and arsenite adsorption and desorption behavior on coprecipitated aluminum: iron hydroxides. *Environ. Sci. Technol.* **41**, 837–842.

Mcbride M. B. and Wesselink L. G. (1988) Chemisorption of catechol on gibbsite, boehmite, and noncrystalline alumina surfaces. *Environ. Sci. Technol.* **22**, 703–708.

Mello J. W. V., Roy W. R., Talbott J. L. and Stucki J. W. (2006) Mineralogy and arsenic mobility in arsenic-rich Brazilian soil and sediments. *J. Soils Sediments* **6**(1), 9–19.

Meng X., Korfiatis G. P., Jing C. and Christodoulatos C. (2001) Redox transformations of arsenic and iron in water treatment sludge during aging and TCLP extraction. *Environ. Sci. Technol.* **35**, 3476–3481.

Monkhorst H. J. and Pack J. D. (1976) Special points for Brillouin-zone integrations. *Phys. Rev. B* **13**, 5188–5192.

Noronha A. L. O., Guimarães L. and Duarte H. A. (2007) Structural and thermodynamic analysis of the first mononuclear aqueous aluminum citrate complex using DFT calculations. *J. Chem. Theory Comput.* **3**(3), 930–937.

Oliveira A. F., Ladeira A. C. Q., Ciminelli V. S. T., Heine T. and Duarte H. A. (2006) Structural model of arsenic(III) adsorbed on gibbsite based on DFT calculations. *J. Mol. Struct.-THEOCHEM* **762**, 17–23.

Oliveira A. F., Seifert G., Heine T. and Duarte H. A. (2009) Density-functional based tight-binding: an approximate DFT method. *J. Braz. Chem. Soc.* **20**, 1193–1205.

Pack J. D. and Monkhorst H. J. (1977) Special points for Brillouin-zone integrations – reply. *Phys. Rev. B* **16**, 1748–1749.

Paktunc D., Dutrizac J. and Gertsman V. (2008) Synthesis and phase transformations involving scorodite, ferric arsenate and arsenical ferrihydrite: implications for arsenic mobility. *Geochim. Cosmochim. Acta* **72**, 2649–2672.

Pantuzzo F. L. and Ciminelli V. S. T. (2010) Arsenic association and stability in long-term disposed arsenic residues. *Water Res.* **44**, 5631–5640.

Ravel B. and Newville M. (2005) Athena, Artemis, Hephaestus: data analysis for X-ray absorption spectroscopy using IFEFFIT. *J. Synchrotron Radiat.* **12**, 537–541.

Rodrigues G. S., Cunha I. S., Silva G. G., Noronha A. L. O., Abreu H. A. and Duarte H. A. (2011) DFT Study of Vanadyl (IV) Complexes with low molecular mass ligands: picolinate, oxalate, malonate, and maltolate. *International Journal of Quantum Chemistry*. **111**, 1395–1402.

Saalfeld H. and Wedde M. (1974) Refinement of crystal-structure of gibbsite, $Al(OH)_3$. *Z. Kristallogr.* **139**, 129–135.

Schaefer C. E. G. , Fabris J. D. and Ker J. C. (2008) Minerals in the clay fraction of Brazilian Latosols (Oxisols): a review. *Clay Mineral.* **43**, 137–154.

Sherman D. and Randall S. R. (2003) Surface complexation of arsenic(V) to iron(III) (hydr)oxides: structural mechanism from ab initio molecular geometries and EXAFS spectroscopy. *Geochim. Cosmochim. Acta* **67**(22), 4223–4230.

Silva J, Mello J. W. V, Gasparon M., Abrahão W. A. P., Jong T. (2007). Arsenate adsorption onto aluminium and iron (hydr)oxides as an alternative for water treatment. In Water in Mining Environments (eds. R. Cidu and F. Frau). IMWA Symposium 2007, Cagliari, Italy.

Silva J., Mello J. W. , Gasparon M., Abrahão W. A. , Ciminelli V. S. T. and Jong T. (2010) The role of Al–Goethites on arsenate mobility. *Water Res.* **44**, 5684–5692.

Vasconcelos I. F., Haack E. A., Maurice P. A. and Bunker B. A. (2008) EXAFS analysis of Cd(II) adsorption to kaolinite. *Chem. Geol.* **249**, 237–249.

Voegelin A., Kaegi R., Frommer J. and Vantelon H. U. G. D. S. J. (2010) Effect of phosphate, silicate, and Ca on Fe(III)-precipitates formed in aerated Fe(II)- and As(III)-containing water studied by X-ray absorption spectroscopy. *Geochim. Cosmochim. Acta* **74**, 164–186.

Weerasooriya R., Tobschall H. J., Wijesekara H. K. D. K., Arachchige E. K. I. A. K. U. K. and Pathirathne K. A. S. (2003) On the mechanistic modeling of As(III) adsorption on gibbsite. *Chemosphere* **51**, 1001–1013.

Weerasooriya R., Tobschall H. J., Wijesekara H. K. D. K. and Bandara A. (2004) Macroscopic and vibration spectroscopic evidence for specific bonding of arsenate on gibbsite. *Chemosphere* **55**, 1259–1270.

Associate editor: William H. Casey